doi:10.1016/j.jmb.2007.09.005 J. Mol. Biol. (2007) 374, 130–146

JMB

Available online at www.sciencedirect.com
ScienceDirect

ELSEVIER

Affinity Maturation Increases the Stability and Plasticity of the Fv Domain of Anti-protein Antibodies

Juan Pablo Acierno[1], Bradford C. Braden[2], Sebastián Klinke[1] Fernando A. Goldbaum[1] and Ana Cauerhff[1]*

[1]*Fundación Instituto Leloir Consejo Nacional de Investigaciones Cientificas y Técnicas de Argentina (IIBBA-CONICET) Buenos Aires, Argentina*

[2]*Department of Natural Sciences, Bowie State University, Bowie, MD, USA*

Received 22 June 2007; received in revised form 13 August 2007; accepted 5 September 2007
Available online
11 September 2007

Edited by I. Wilson

The somatic mutations accumulated in variable and framework regions of antibodies produce structural changes that increase the affinity towards the antigen. This implies conformational and non covalent bonding changes at the paratope, as well as possible quaternary structure changes and rearrangements at the V_H–V_L interface. The consequences of the affinity maturation on the stability of the Fv domain were studied in a system composed of two closely related antibodies, F10.6.6 and D44.1, which recognize the same hen egg-white lysozyme (HEL) epitope. The mAb F10.6.6 has an affinity constant 700 times higher than D44.1, due to a higher surface complementarity to HEL. The structure of the free form of the Fab F10.6.6 presented here allows a comparative study of the conformational changes produced upon binding to antigen. By means of structural comparison, kinetics and thermodynamics of binding and stability studies on Fab and Fv fragments of both antibodies, we have determined that the affinity maturation process of anti-protein antibodies affects the shape of the combining site and the secondary structure content of the variable domain, stabilizes the V_H–V_L interaction, and consequently produces an increase of the Fv domain stability, improving the binding to antigen.

Keywords: affinity maturation; V_H–V_L interface; antibody stability; heat capacity changes; antibody structure

Introduction

During the evolution of the humoral immune response, the affinity maturation process is necessary to improve and refine antibody binding towards the antigen that triggered that particular response.[1,2] Theoretically, by means of somatic mutations accumulated in variable region of antibodies, a great variety of structural changes can be produced, thereby increasing the affinity towards the specific antigen. All these changes point to improvement of the binding site complementarity towards the antigen, by several mechanisms e.g. through water-mediated contacts between antigen and antibody,[3] hypervariable loop conformation changes,[4] and rotation of the variable domain of the heavy chain (V_H)–variable domain of the light chain (V_L) interface[5] among others. However, an affinity ceiling of 10^{10} M^{-1} was described,[6,7] thus, higher affinity in activated lymphocyte clones does not seem to produce an advantage in competition for the antigen.

Numerous studies have described the molecular basis of the affinity maturation of antibodies against haptens.[8–12] Using the hapten model, affinity maturation is understood as a process of accumulation of mutations favored by long-term exposure to antigen in the production of high-affinity antibodies. Some authors have described two distinct antibody maturation pathways in this immune response, each pathway involves antibodies having high affinity for the antigen with a slow maturation or having medium affinity for the antigen with a rapid

*Corresponding author. E-mail address: acauerhff@leloir.org.ar.

Abbreviations used: HEL, hen egg-white lysozyme; mAb, monoclonal antibody; CDR, complementarity-determining region; FR, framework region; V_H, variable domain of the heavy chain; V_L, variable domain of the light chain; Fab, antigen-binding fraction; Fv, variable fraction; C_H1, first constant domain of the heavy chain; C_L, constant domain of the light chain; rmsd, root-mean-square deviation; vdW, van der Waals; ANS, 8-anilino-1-naphthalenesulfonic acid.

maturation.[13] Junctional amino acids in $CDR3_H$ would have a significant role in determining the evolvability of antibodies.[13] Structurally, affinity maturation results from an increase in surface complementarity (SC), as a consequence of a finely tuned process chaperoned by the somatic mutations, implying a more efficient hapten-induced fit in the mature antibody.[11] However, there is evidence that the flexibility of the binding pocket decreases in concert with gains in affinity[14] and is associated with a decreased entropic cost to binding.[15]

In the immune response against a typical T-dependent protein antigen, the affinity maturation process is fast and is associated with the early class switch event from IgM to IgG. The time of exposure to the antigen does not improve the average binding affinity and association constant (k_{ass}) of the antibodies generated during anti-protein secondary immune response.[16] It is important to emphasize that the results obtained from anti-hapten antibodies cannot be expected to extrapolate to antibodies directed against protein antigens because antibody–protein interfaces bury a surface at least three times larger than antibody–hapten and involved two to three times more contacts. Thus, the affinity maturation process for anti-protein antibodies is more complex, and it is possible that the structural basis of this process is not a single pathway. The study of the affinity maturation of D1.3, an antibody specific for hen egg-white lyzozyme (HEL), showed that the replacement mutations were antigen-selected and situated mainly in the complementarity-determining regions (CDRs). The affinity maturation leading to antibody D1.3 appeared to be exclusively due to a decrease in the rate of dissociation (k_{diss}) of the complex with HEL.[2] In another study, comparing the structure of four antibodies that recognize an overlapping epitope of HEL, different from that recognized by D1.3, it was observed that the binding is enhanced by the increasing amount of apolar surface at the periphery of the interface with antigen, producing an improved shape complementarity towards HEL. The antibodies showed an overall correlation between affinity and the number of somatic mutations, but no correlation with hydrogen bonds and van der Waals (vdW) contacts between HEL and the antibodies,[17] which are the major contributors to affinity maturation in anti-hapten responses.[18]

Although it is known that antibody–protein interactions can imply conformational changes in the paratope, there is little information about the conformational rearrangements produced at the V_H–V_L interface due to complex formation in the literature. Some examples of quaternary rearragements and conformational changes at that interface in antibody–protein complexes have been reported.[19] Moreover, crystallographic structure comparison of antigen-binding fraction (Fab) and variable fraction (Fv) fragments of D1.3, showed that small rearrangements are made at the Fv, bridging the contacting residues closer to the antigen as compared to the Fab fragment, indicating an induced-fit mechanism to bind HEL.[20] Other examples show that the Fv fragment can undergo local structural rearrangements in V_H domain and a different water distribution at the V_H–V_L interface from that found in the Fab fragment upon binding to antigen.[21,22] Earlier studies suggest that the unfavorable effect of deletion of constant regions on the stability of Fv fragment[23] is sometimes compensated by an increase in favorable interactions of this fragment towards the antigen.[21] Furthermore, studies regarding the stability of different antibody domains show that the mutual stabilization occurs across the V_H–V_L and first constant domain of the heavy chain (C_H1) – constant domain of the light chain (C_L) interfaces indicating a high degree of cooperation.[23] The antibody Fv assembly is a cooperative process requiring a coupled folding and domain association, as the V_H–V_L interaction is crucial in folding and stabilizing the Fv domain.[24] For biotechnological purposes, re-engineering the V_H–V_L interface of antibodies could be useful to improve the stability, refolding efficiency and the affinity towards antigen of Fv and single-chain Fv (scFv) antibodies.

In this work, we studied the effect of the antibody affinity maturation process on the improvement of the complementarity towards the antigen, especially focusing on the conformational changes at the V_H–V_L interface produced upon complex formation. In addition, the relationship between affinity maturation and stability of the Fv domain was explored using several approaches. As a model, we used two murine monoclonal antibodies (mAbs) that recognize the same β pleated sheet domain of HEL.[25] These two mAbs are sequence and structure-related, since their V_H and V_L are derived from the same rearrangement of germline genes, although they are the product of different immunization protocols. The V_H of both antibodies seems to accumulate more mutations in FRs than in CDRs, especially V_H F10.6.6, which accumulates 13 mutations in FRs. A comparative study between these two antibodies showed that mAb F10.6.6 has a ~700 times greater affinity towards HEL than mAb D44.1. Thus, the increased number of somatic mutations in mAb F10.6.6 correlates with the increase in affinity towards the antigen. Recently, the three-dimensional structure of a Fab fragment of F10.6.6 in complex with HEL was described.[26] The comparison of the crystallographic structures of both antibody complexes suggests that they are the product of different degrees or different pathways of affinity maturation, and reveals that this process produces a fine-tuning of the complementarity of the antigen combining site towards the epitope. The number of non-covalent bonds (vdW, hydrogen bonds and ion pairs) increases significantly from 93 in D44.1 to 129 in the F10.6.6 complex, besides F10.6.6 forms closer and stronger bonds with HEL than D44.1. In agreement with these results, F10.6.6-HEL shows an improvement of SC, this fact and the extra water molecule between F10.6.6 and HEL can explain the difference in enthalpy of reaction between F10.6.6 and HEL compared with D44.1-

HEL.[26] All these findings suggest that the D44.1-F10.6.6 system produces similar affinity maturation mechanism to anti-hapten responses,[10,27,28] but with the changes affecting a larger planar surface.

Along with the free and bound forms of Fab D44.1 reported earlier,[25] the structure of the free form of the Fab F10.6.6, presented here, allow us to make a comparative study about the conformational changes produced upon binding to antigen. Structural analysis, kinetics and thermodynamics of binding and stability studies on Fab and Fv fragments of both antibodies are presented here. This integral study leads us to conclude that the affinity maturation process of these two antibodies affects the shape of the combining site and increases the stability of the Fv domain.

Results

Binding kinetics and thermodynamics of the Fab and Fv fragments of mAbs D44.1 and F10.6.6

As described,[26] the Fab F10.6.6 has a ~700-fold higher affinity towards HEL than Fab D44.1, with k_{ass} about 170-fold faster and k_{diss} about fourfold slower. In order to gain a deeper insight into the molecular basis that governs the binding process of the paratope of both antibodies towards HEL, we investigated the antigen binding of their respective recombinant Fv fragments. The use of Fv fragments allows us to examine the contribution of the accumulated mutations in the variable region (Figure 1) without constraint of the stabilizing forces of the constant domain.[26]

Table 1 shows that the kinetic and thermodynamic behavior of the Fab and Fv fragments of D44.1 and F10.6.6 antibodies follow different trends. On one hand, Fv D44.1 presents faster k_{ass} and k_{diss} than its parent Fab fragment. This compensation results in the Fab and Fv fragments having nearly identical affinity constants (K_A) towards HEL. In contrast, Fv F10.6.6 has slower k_{ass} and faster k_{diss} than its parent Fab fragment, which results in a decrease of one order of magnitude in K_A.

In most cases reported, antibody Fv fragments show lower affinity than their Fab counterparts because of a loss of stability due to the lack of the constant domains.[20] Thus, F10.6.6 seems to follow the rule, while D44.1 seems to be the exception. However, the thermodynamic analysis shows that both Fv fragments present a similar proportional decrease in binding enthalpy compared to their respective Fab fragments.

The Fab and Fv F10.6.6-HEL reactions follow the same thermodynamic tendency as found for other Fab-HEL reactions, i.e. they are enthalpically driven with large unfavorable entropy. Conversely, the Fab and Fv D44.1-HEL reactions are enthalpically driven with almost no entropy compensation. These small changes in the kinetics and thermodynamics behavior of the Fab and Fv fragments prompted us to examine the structural aspects that could explain these relationships and their potential relevance to the affinity maturation process.

Structural analysis of free and bound Fab D44.1 and F10.6.6 antibodies

In order to study potential conformational changes and water rearrangements produced at

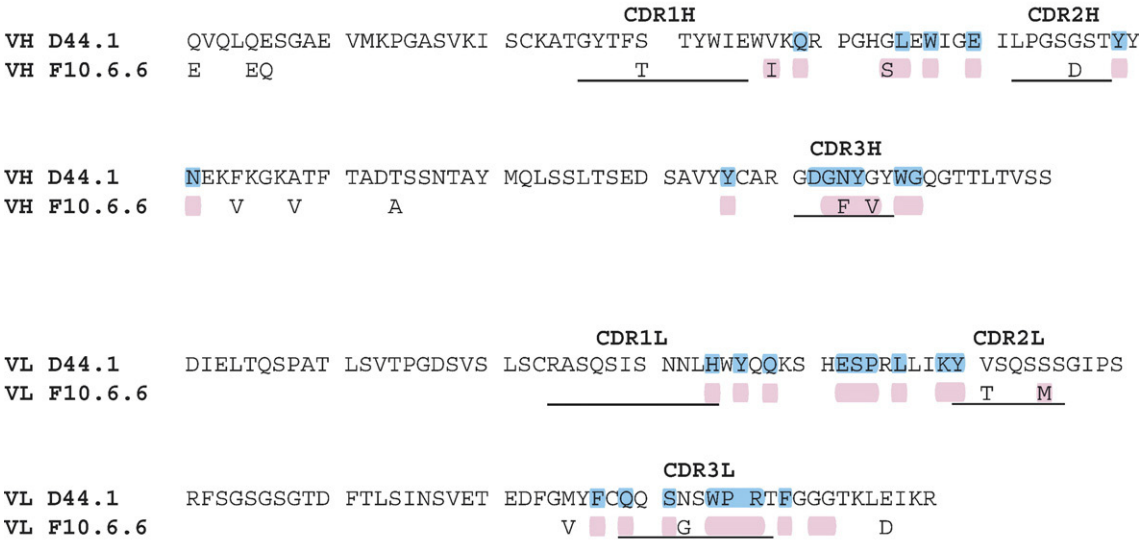

Figure 1. Sequence alignment of the variable region of mAbs D44.1 and F10.6.6. Amino acid sequences of V_H D44.1, V_H F10.6.6, V_L D44.1, and V_L F10.6.6. Assignment of antibody CDRs follows the AbM definition, based on sequence variability (Kabat definition[69,70]) and the location of the structural loop regions (Chothia definition[71]). CDR residues are underlined in both sequences. Residues comprising the V_H–V_L interface of the free antibody structures are represented as cyan squares for D44.1 and pink squares for F10.6.6.

Table 1. Binding kinetics and thermodynamics of Fv and Fab fragments of mAbs F10.6.6 and D44.1 with HEL at 25 °C

Antibody	k_{ass}[a] (M^{-1} s^{-1})	k_{diss}[a] (s^{-1})	K_A[a] (M^{-1})	ΔG^{ob} (kcal mol^{-1})	$\Delta H°$ (kcal mol^{-1})	$-T\Delta S^{ob}$ (kcal mol^{-1})
Fab F10.6.6	$7.19(\pm 0.02)\times10^{6}$	$7.00(\pm 0.09)\times10^{-4}$	$1.02(\pm 0.13)\times10^{10}$	−13.52	−18.25±0.81[c]	−4.53
Fv F10.6.6	$1.12(\pm 0.07)\times10^{6}$	$1.00(\pm 0.02)\times10^{-3}$	$1.12(\pm 0.07)\times10^{9}$	−12.37	−15.72±0.06	−3.35
Fab D44.1	$4.21(\pm 0.55)\times10^{4}$	$2.92(\pm 0.01)\times10^{-3}$	$1.44(\pm 0.13)\times10^{7}$	−9.67	−10.34±0.45[c]	−0.67
Fv D44.1	$7.10(\pm 0.52)\times10^{4}$	$5.44(\pm 0.004)\times10^{-3}$	$1.30(\pm 0.09)\times10^{7}$	−9.69	−9.17±0.18	0.52

[a] Determined by IAsys biosensor for Fvs (this work) and for Fabs (taken from Cauerhff *et al.*[26]).
[b] Calculated from the equations $\Delta G° = -RT\ \mathrm{In}K_A$ and $\Delta G° = \Delta H° - T\Delta S°$.
[c] Taken from Schwarz *et al.*[47]

the combining site and V_H–V_L interface of Fab F10.6.6 upon binding to HEL, the free Fab fragment was crystallized in the same condition than the Fab F10.6.6-HEL complex, but its crystals belong to a different crystallographic space group than those of the complex.[26] The structure was solved by the molecular replacement method using the Fab fragment of the latter complex (PDB code 1P2C) as a search model. Two molecules were found in the asymmetric unit. As the structures of both free and bound Fab D44.1 have been reported,[25] we can compare the kinetics and thermodynamics of binding of both antibodies with their respective free and bound crystallographic structures.

Overall structural comparison

The study of atomic position shifts in proteins is known to fall into two categories: first, concerted movements of the peptide backbone; and second, changes in the orientations of the side-chains. For studying the first category of movements we superimposed all C^{α} of Fab, Fv, V_H and V_L domains between free and bound species of F10.6.6 and D44.1 using a a least-squares procedure (Table 2). The root-mean-square deviation (rmsd) values from F10.6.6 are higher than for D44.1, especially when Fv domains are superimposed, because of the sum of quaternary and tertiary changes at the overall structure.

Table 2. Structural alignment of Fab, Fv, V_H and V_L free and bound domains from mAbs F10.6.6 and D44.1

Domain	F10.6.6	D44.1
Fab	0.90	0.83
Fv	0.84	0.62
V_H	0.91	0.60
V_L	0.50	0.38
$FR1_H$	0.40	0.40
H1	0.48	0.83
$FR2_H$	1.21	0.69
H2	0.78	1.40
$FR3_H$	1.14	0.36
H3	0.52	0.83
$FR4_H$	0.41	0.32
$FR1_L$	0.48	0.55
L1	0.42	0.36
$FR2_L$	0.20	0.26
L2	0.64	0.45
$FR3_L$	0.48	0.41
L3	0.43	0.60
$FR4_L$	0.36	0.41

The results are given as rmsd (in Å) taking into accounts the C^{α} atoms and all structures found in the asymmetric unit.

Quaternary changes in the relative orientation of the V_H and V_L domains between the free and bound structures of F10.6.6 were analyzed by superimposing the corresponding V_L domains from free and bound antibodies and then by determining the rotations and translations to superimpose their V_H domains. For Fab F10.6.6, the rotation and translation to superimpose V_H are 2.9° and 1.1 Å, respectively. A similar rotation value was found for Fab D44.1 structures (3.0°) but translation was very small and less than the rmsd error in atomic position.[25] According to these results, for both antibodies the consequence of HEL binding is a subtle shifting of the V_H β-strands relative to V_L, but for Fv F10.6.6 this effect is more evident (see section V_H–V_L interface, below).

The rmsd values observed in Fv domains between the free and antigen-bound forms of F10.6.6 and D44.1 highlight the tertiary conformational changes of the V_H domain, especially for F10.6.6 (Table 2). Higher rmsd values are found in framework regions $FR2_H$ and $FR3_H$ for F10.6.6. In contrast, D44.1 shows small changes along V_H, including CDR_H2 and CDR_H3 regions. These differences in FR regions are mainly due to the backbone movement and are consistent with more mutations in F10.6.6 with respect to germline sequence. These comprise the displacement of two protein segments at V_H; first, a significant movement was found in the segment between the residues $Arg40_H$ and $Leu45_H$ ($FR2_H$), producing a shift of about 4 Å in the backbone. Second, another backbone dislocation was found in the segment between $Asn61_H$ and $Lys67_H$ ($FR3_H$) where the main chain twisted in the opposite direction with a maximum displacement of 4.5 Å. For Fab D44.1 small conformational changes in all Fv domain are observed, and backbone displacements in FR regions are noticed but to a lesser extent, producing a displacement of 2.5 Å and 1.5 Å in $FR2_H$ and $FR3_H$, respectively. In this fashion, V_H F10.6.6 seems to be more compact with large conformational changes upon binding to HEL only at $FR2_H$ and $FR3_H$. In contrast, with Fv D44.1 exhibits small conformational changes along all the V_H structure, suggesting a less stable organization. The V_L F10.6.6 domain also undergoes small conformational changes confined at $CDR3_L$. Backbone displacement of $Gly92_L$ affects $Ser93_L$ and $Trp94_L$ side-chains orientation.

In summary, the conformational changes of Fab F10.6.6 upon binding to HEL reflect that the profound backbone displacements are less apparent in CDRs, and the conformational changes in residues that form the paratope are restricted to side-chains. Conversely, for D44.1 the conformational changes of the CDRs involve both backbone and side-chain shifts. The presence of water molecules at the binding interface was studied in all structures. Since the structures of the Fab F10.6.6 in the free and bound form were solved at higher resolution than the Fab D44.1 structures, more water molecules are observed. However, considering the *B*-factors of water molecules in all structures, a displacement of an average of four water molecules (forming hydrogen bonds) is observed between free and bound forms in both antibodies.

Since the more evident effects of antigen binding on the overall structure of Fab F10.6.6 are the quaternary changes i.e. the relative orientation of the V_H and V_L domains, a detailed analysis of the V_H–V_L interface was performed.

V_H–V_L interface

The differences in buried surface area (*BSA*) at the V_H–V_L interface in the free and bound forms of Fab F10.6.6 and D44.1 are not significant (25 Å^2 and 9 Å^2, respectively). However, the *BSA* of free Fab F10.6.6 V_H–V_L interface is 8% higher than that of free Fab D44.1 (1527 Å^2 *versus* 1412 Å^2). When the SC of the V_H–V_L interface is analyzed (Table 3), Fab F10.6.6 shows a significantly higher value (39%) than Fab D44.1, implying a more pronounced interaction between the V_H and V_L domains. In addition, no significant difference is found between free and bound forms in the Fab F10.6.6. In contrast, there is a difference of 19% in the SC at the V_H–V_L interface in the free and bound forms of Fab D44.1, suggesting that this interface tightens upon binding to antigen.

The residues that comprise the V_H–V_L interface of the unliganded form of both Fab F10.6.6 and D44.1 are represented in Figure 1 as light blue and pink boxes, respectively. It can be observed that there are more residues comprising that interface in F10.6.6 than in D44.1. Also, the number of intermolecular contacts at the V_H–V_L interface of the unliganded form of Fab F10.6.6 is 37% higher than that found for free Fab D44.1 (Table 3), which is in agreement with *BSA* and SC analyses. However, it is noteworthy that both antibodies present a similar number of contacts in the bound form (119 *versus* 115 contacts). Thus, upon binding to HEL, the V_H–V_L interface in Fab F10.6.6 loses 41 vdW contacts and gains two hydrogen bonds, which indicates that a noticeable V_H–V_L rearrangement occurs upon binding. In contrast, the interface in Fab D44.1 loses only eight vdW contacts and gains two hydrogen bonds during binding to the antigen. Analyzing all the results expressed in Table 3, it can be argued that upon binding to HEL, the V_H–V_L interface in Fab D44.1 undergoes local rearrangements losing 20 contacts from FR_H–CDR_L and two from CDR_H–FR_L, but gaining ten contacts from FR_H–FR_L and six from CDR_H-CDR_L. In this fashion, a net loss of only six contacts at the V_H–V_L interface is allowed for D44.1 upon binding to HEL without affecting the Fv domain stability. On the other hand, the net loss of 39 contacts at the V_H–V_L interface in Fab F10.6.6 is

Table 3. Atomic contacts and surface complementarity (SC) of the V_H–V_L interface of free and bound Fab fragments from mAbs F10.6.6 and D44.1

	Fab D44.1								
	Free			Bound			Δ (Bound–Free)		
	H-bond	vdW	Total	H-bond	vdW	Total	H-bond	vdW	Total
VH-VL	6	115	121	8	107	115	2	−8	−6
FR_H-FR_L	2	26	28	4	34	38	2	8	10
FR_H-CDR_L	2	39	41	1	20	21	−1	−19	−20
CDR_H-FR_L	1	20	21	1	18	19	0	−2	−2
CDR_H-CDR_L	1	30	31	2	35	37	1	5	6
$CDR3_H$-$CDR3_L$	1	15	16	1	16	17	0	1	1
SC			−93.1			−114.8			−21.7
	Fab F10.6.6								
	Free			Bound			Δ (Bound – Free)		
	H-bond	vdW	Total	H-bond	vdW	Total	H-bond	vdW	Total
VH-VL	7	151	158	9	110	119	2	−41	−39
FR_H-FR_L	5	51	56	5	39	44	0	−12	−12
FR_H-CDR_L	0	34	34	1	22	23	1	−12	−11
CDR_H-FR_L	1	30	31	1	20	21	0	−10	−10
CDR_H-CDR_L	1	36	37	2	29	31	1	−7	−6
$CDR3_H$-$CDR3_L$	1	17	18	1	12	13	0	−5	−5
SC			−130.2			−126.5			3.7

Atomic contacts were calculated for both crystallographic structures in the asymmetric unit of each antibody using a cutoff of 4.0 Å. Higher absolute values of SC means more complementarity. Surface complementarity values were calculated with FADE software.[68]

the result of the loss of non-covalent contacts from all regions of that interface analyzed. Remarkably, about 50% of the total contacts lost upon binding to HEL in Fab F10.6.6 are located in the $FR2_H$ ($Ile37_H$, $Gln39_H$, $Ser44_H$ $Leu45_H$, $Trp47_H$ and $Glu50_H$) and in $CDR3_L$ ($Gln89_L$, $Ser91_L$, $Trp94_L$, $Pro95_L$ and $Arg96_L$).

A detailed analysis of the conservation of individual intermolecular contacts at the V_H–V_L interface indicates that in Fab F10.6.6, of 158 contacts found in the free form, 96 are conserved upon binding (61%), including six hydrogen bonds. As such, 23 new contacts including three hydrogen bonds are formed, giving a total of 119 contacts for the bound form. For Fab D44.1, 69 contacts (57%) from 121 found in the free form are conserved in the bound form, including four hydrogen bonds. Thus, 46 new contacts are formed at the V_H–V_L interface upon binding of antigen. A significant structural change found at the V_H–V_L interface of bound Fab F10.6.6 is produced when HEL pushes $Glu35_H$ towards V_L, producing a displacement of 2.3 Å of its side-chain and originating four contacts with V_L. In this way, $Glu35_H$ O^{ε} forms a hydrogen bond with $Arg96_L$ N^{ε}, which would help to position $Glu35_H$ to stabilize the salt-bridge with Arg68 of HEL.[26] The results summarized in Tables 2 and 3 highlight that conformational changes upon binding are more apparent in F10.6.6 than in D44.1.

Figure 2 shows the surface of the V_H domains of antibodies F10.6.6 and D44.1, highlighting the atoms that contact the V_L domain and the location of the most important conformational changes occurred upon binding to the antigen. Figure 2 demonstrates that the residues of V_H F10.6.6 with higher rmsd

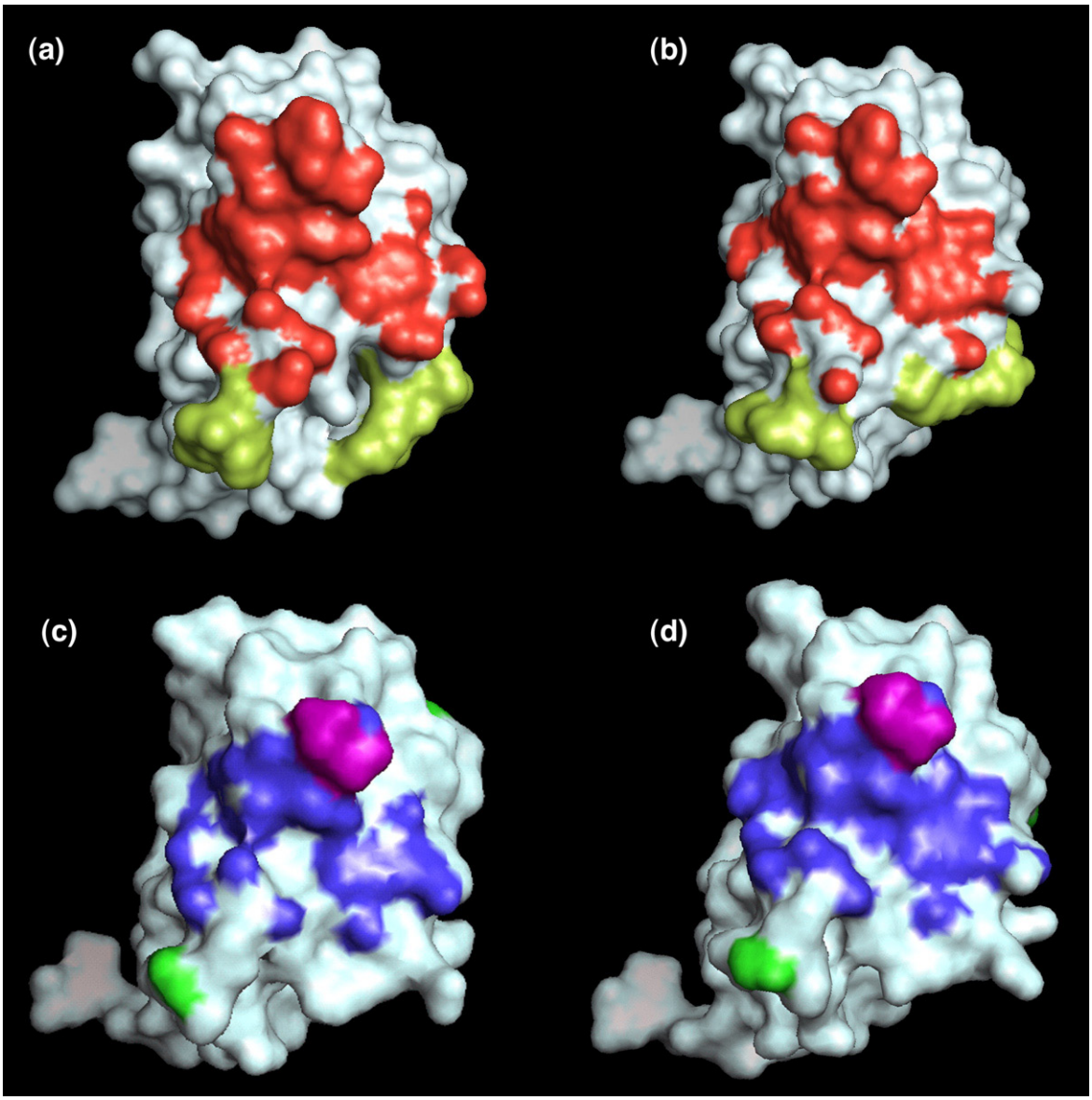

Figure 2. Changes at the V_H–V_L interface upon binding to HEL. The V_H surface is depicted, highlighting the residues that contact V_L. (a) Free and (b) bound V_H F10.6.6. V_H–V_L contacts are in red and residues with high rmsd values are in light green. (c) Free (d) bound V_H D44.1. V_H–V_L contacts are in blue, residues with high rmsd values outside the interface are in green and those inside the interface are in purple.

values (superimposing free and bound V_H F10.6.6) are outside the V_H–V_L interface ($Gly42_H$, $His43_H$, $Glu62_H$, $Val64_H$ and $Lys65_H$). These residues constitute the two segments at $FR2_H$ and $FR3_H$ that undergo backbone displacements described in the previous section. For D44.1, fewer contacts are noticed at the V_H–V_L interface (Table 3; Figure 2). The residues having higher rmsd values are inside ($Asp100_H$, $Gly101_H$ and $Asn102_H$) and outside the V_H–V_L interface ($Gly42_H$, $Gly54_H$ and $Gly56_H$). In summary, the dislocations in the main chain of the V_H F10.6.6 would permit an internal rearrangement in order to maintain the binding to V_L and thus, the stability of F10.6.6 would not be weakened because of binding to HEL. The results summarized in Tables 2 and 3, and in Figure 2 argue that free F10.6.6 is more plastic to accommodate rearrangements of the V_H–V_L interface during binding to HEL while, on the other hand, D44.1 appears unable to accommodate the large conformational changes required to improve the binding to the antigen. Moreover, the analysis of *BSA* values, interface complementarity and the atomic contacts of the free forms of both antibodies, demonstrates that the V_H–V_L interaction is stronger in F10.6.6 than in D44.1, suggesting that F10.6.6 Fv domain is more stable than that from D44.1.

Thermal stability of antibody fragments studied by circular dichroism and dynamic light-scattering

In order to study the stability of the Fv fragments and the contribution of the constant domain in Fv stabilization we have analyzed the secondary structure content of the Fab fragments by spectroscopy in solution and by analysis of the crystal structures with the DSSP program.[29] For recombinant Fv fragments, we performed only the spectroscopy studies, since the crystal structures are not available.

Native circular dichroism (CD) spectra of Fab and Fv fragments from F10.6.6 and D44.1 were obtained in PBS buffer at 20 °C and show a typical β-structure signal (see the insets in Figure 3(a) and (b), respectively) with positive peaks at 203 nm and 233 nm, and a negative peak at 216 nm. This type of CD spectra is commonly observed studying

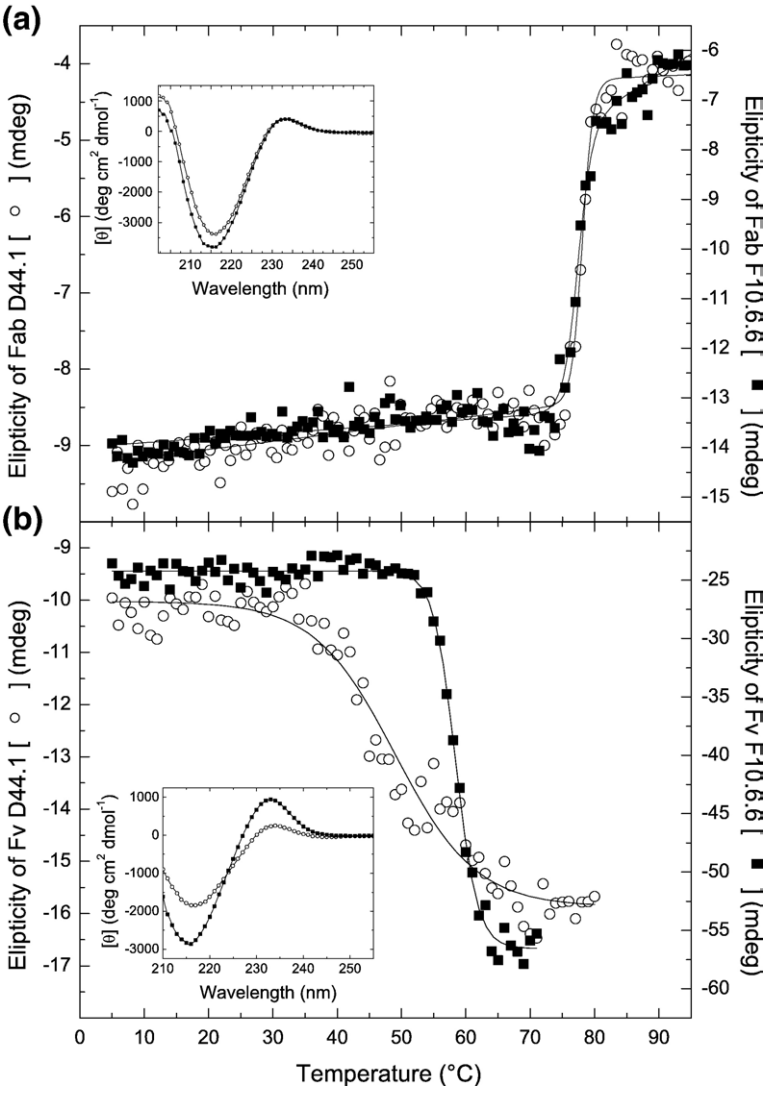

Figure 3. Thermal denaturation of (a) Fab and (b) Fv fragments, following the signal of β-sheet structure at 216 nm. F10.6.6 is represented with filled squares and D44.1 with open circles. The far-UV CD spectra of both Fabs and Fvs, plotting molar elipticity as a function of wavelength, are shown as insets.

antibody fragments and it is attributed to the environment of aromatic residues.[30–34] Thus, the spectra of both antibodies Fab fragments (Figure 3(a), inset) present nearly the same content of β-sheet structure. However, although the spectra of the Fv fragments are typical of proteins with high content of β structure, they differ in amplitude at 216 nm and 233 nm (Figure 3(b), inset). Since the amplitude of far-UV CD in immunoglobulins is influenced by aromatic amino acid content and disulfide bridges,[31,35] it is difficult to calculate accurately the secondary structure of an antibody. For this reason, we used the objective method discussed by Tetin *et al.*[34] to evaluate the secondary structure content in the antibody fragments. As such, secondary structure is calculated from far-UV CD data using three different methods and two sets of proteins.[36] Consequently, structural and CD analysis showed that both Fab fragments have overall the same content of secondary structure (results not shown; see Supplementary Data Table A).

The CD spectra analysis of the Fv fragments of both antibodies (Table 4) showed that the Fv D44.1 is less β-structured than Fv F10.6.6, with a more disordered structure (18.5%) than the Fv F10.6.6. The latter presents more β-sheet (12.9%) and more turn structure content (18.5%). This difference in secondary structure content of the Fv fragment could mean a decrease of thermodynamic stability for Fv D44.1. The study of thermal denaturation (or unfolding) of Fab and Fv fragments by CD spectra, following the loss of β-sheet structure at 216 nm and at 233 nm (data not shown), is outlined in Figure 3(a) and (b), respectively.

In all cases, the protein solution leads into an irreversible aggregation when heated; thus, the melting point (T_m) values are apparent and can be defined as a 50% change in CD signal at 216 nm. For Fv D44.1, a smaller and partially cooperative change in CD signal appears, suggesting the possibility of an unfolding intermediate state[37] or an alternative path of unfolding. For Fv F10.6.6, in contrast, a sharp transition with a thermal unfolding cooperativity is observed (Figure 3). Thermal denaturation of both Fab fragments show a sharp transition at 77 °C (Figure 3(a)). Dynamic light-scattering experiments (DLS) were performed to calculate T_m values as a complement of CD. Thermal denaturation was followed as the change in intensity measured as count rates (CRs) in the temperature range from 30 °C to 90 °C for the Fab and Fv fragments (Figure 4(a) and (b), respectively). Thus, an increase in CRs as the temperature increases represents protein denaturation followed by aggregation and as was described for CD experiments, the apparent T_m can be defined as a 50% change of dispersion intensity (Table 5). Direct comparison of T_m values obtained from CD and DLS is not advisable due to the different temperature rates used in the two methods. Temperature rates are set as 2 deg.C per minute in CD measurements and 1 deg.C per minute for DLS to assure good statistic parameters. However, both datasets obtained by CD and DLS follow the same trend. For Fv D44.1, apparent T_m values are lower than for Fv F10.6.6, and both D44.1 and F10.6.6 Fab fragments present the same apparent T_m, which demonstrates a strong stabilization effect that the constant domains exert over the Fvs. Therefore, we can classify these antibody fragments according to thermal stability as follows:

$$\text{Fab D44.1} = \text{Fab F10.6.6} > \text{Fv F10.6.6} > \text{Fv D44.1}$$

Chemical denaturation followed by tryptophan intrinsic fluorescence

In addition to thermal stability, the chemical unfolding/denaturation of the Fab and Fv fragments was investigated by fluorescence, using guanidinium chloride and urea as denaturants.

Since all tryptophan residues are conserved between Fab and Fv fragments of mAbs D44.1 and F10.6.6, it can be assumed that their localization is the same in both recombinant Fvs. The fluorescence center of mass (CM) for the native state (no urea) reflects average changes in the environment of Trp residues present in each Fab or Fv molecule. In the case of the Fab fragments, such a difference is not significant (Figure 5(a)); however, both Fv fragments do not present the same native fluorescence CM, suggesting that the average Trp residues have a different environment in each Fv (Figure 5(b)). The Trp residues in Fv F10.6.6 seem to be less exposed to water molecules than the average Trp residues of Fv D44.1. As can be appreciated in Figure 5(a), both Fab fragment present a similar midpoint of unfolding ($D_{[50]}$ = 3.0 M and 3.2 M, respectively) with similar transition cooperativity. On the other hand, a cooperative unfolding transition can be observed for Fv F10.6.6 ($D_{[50]}$ = 3.0 M) but not for Fv D44.1 (Figure 5(b)). Again, the Fab fragments show similar

Table 4. Secondary structure of F10.6.6 and D44.1 Fv fragments derived from far-UV CD spectrum

		$H_{regular}$	$H_{distorted}$	H_{total}	$S_{regular}$	$S_{distorted}$	S_{total}	*Turn*	*Unordered*
Fv F10.6.6	CD	0.004	0.025	0.029	0.268	0.158	0.426	0.248	0.297
	SD	0.005	0.010		0.019	0.016		0.036	0.049
Fv D44.1	CD	0.006	0.015	0.021	0.243	0.128	0.371	0.202	0.361
	SD	0.005	0.007		0.031	0.008		0.010	0.022

$H_{regular}$ or $S_{regular}$, fraction of residues in the central part of helical segments or strands; $H_{distorted}$ or $S_{distorted}$, fraction of terminus residues in helices (two at each end of the helix; four per helical segment) or β strands (one residue at each end of the strand; two per strand), H_{total} or S_{total} combines fractions of regular and distorted helices or strands.[24]

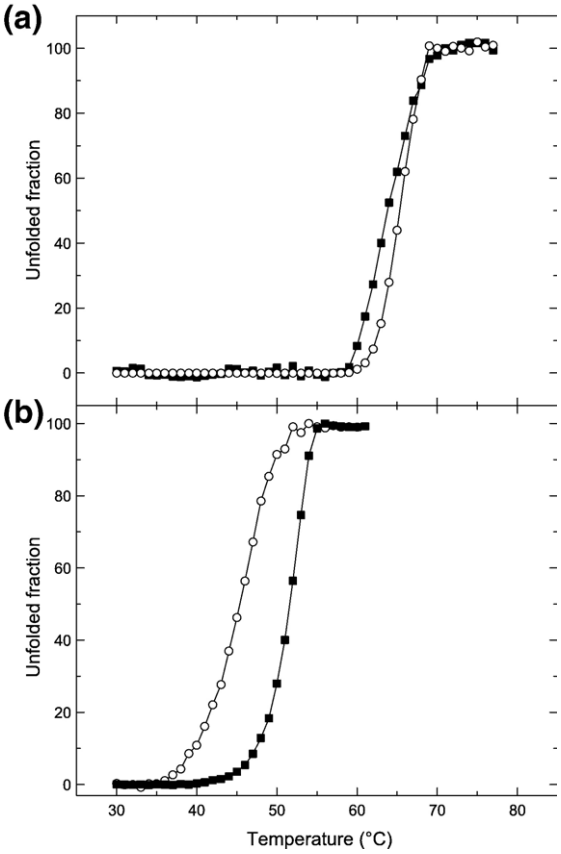

Figure 4. Thermal denaturation of (a) Fab and (b) Fv fragments, following the signal of DLS. F10.6.6 is represented with filled squares and D44.1 with open circles. The data shown are represented as unfolded fraction as a function of temperature.

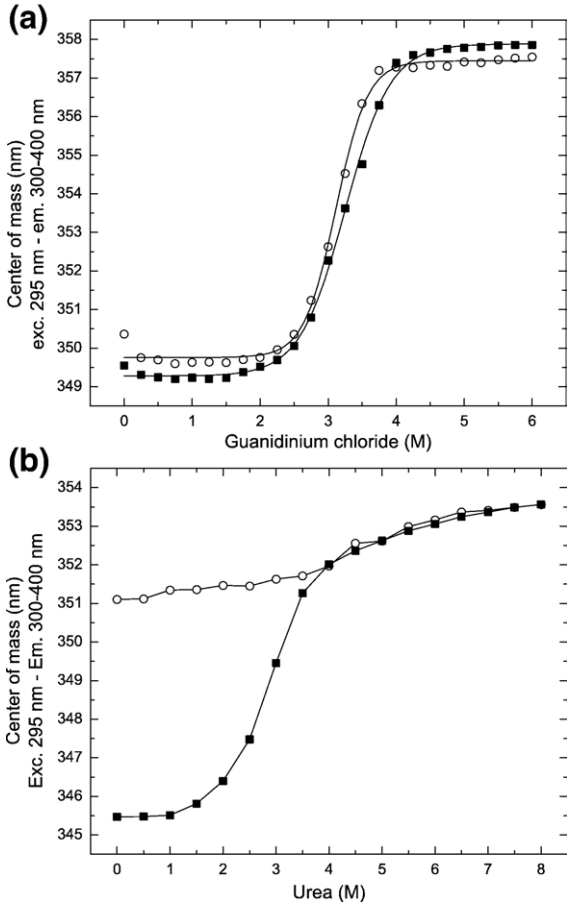

Figure 5. Equilibrium unfolding experiments followed by tryptophan intrinsic fluorescence. (a) Fab fragments denaturation in guanidinium chloride. (b) Fv fragments denaturation in urea. D44.1 and F10.6.6 are represented as open circles and filled squares, respectively. Different native fluorescence CM in both Fvs is noticeable.

stability but Fv F10.6.6 is more stable than Fv D44.1 (Figure 5(b)), which does not present a cooperative unfolding transition. As in the case of the thermal stability studies described above, we can classify these antibody fragments according to their chemical stability as follows:

$$\text{Fab D44.1} = \text{Fab F10.6.6} > \text{Fv F10.6.6} > \text{Fv D44.1}$$

8-Anilino-1-naphthalenesulfonic acid (ANS) binding experiments

When ANS binds to solvent-exposed hydrophobic patches, its quantum yield is enhanced and the maximum of emission is shifted from 520 nm to 480 nm.[38,39] ANS binding is used to monitor the extent of exposure of hydrophobic regions, and to detect non-native partially folded conformations.[28] This probe is known to bind more effectively to the protein in a partially folded state than to a fully folded or unfolded state.[40] Thus, we measured the emission spectra of Fv and Fab fragments in the presence of ANS, in native conditions and with increasing concentrations of urea. The emission spectra of PBS and 8 M urea solutions in the presence of ANS were measured as controls.

The ANS emission spectrum of the Fv F10.6.6 in PBS (Figure 6(a)) has no significant difference with respect to the control experiment, showing that it does not bind ANS. Conversely, the Fv D44.1 spectrum in PBS shows an enhanced emission and its CM is shifted towards the blue, a typical behavior of proteins that bind this probe.[40] The spectra of the Fv fragments of both antibodies in the presence of 8 M urea were nearly equivalent; the loss of tertiary structure and of their ability to bind ANS was observed. Conversely, no binding to ANS was ob-

Table 5. Thermal denaturation studies

Antibody fragment	CD T_m (°C)	DLS T_m (°C)
Fab F10.6.6	77.2	64.0
Fab D44.1	77.4	65.3
Fv F10.6.6	58.4	51.4
Fv D44.1	49.5	44.2

Apparent T_m of antibody fragments were calculated from CD and DLS experiments.

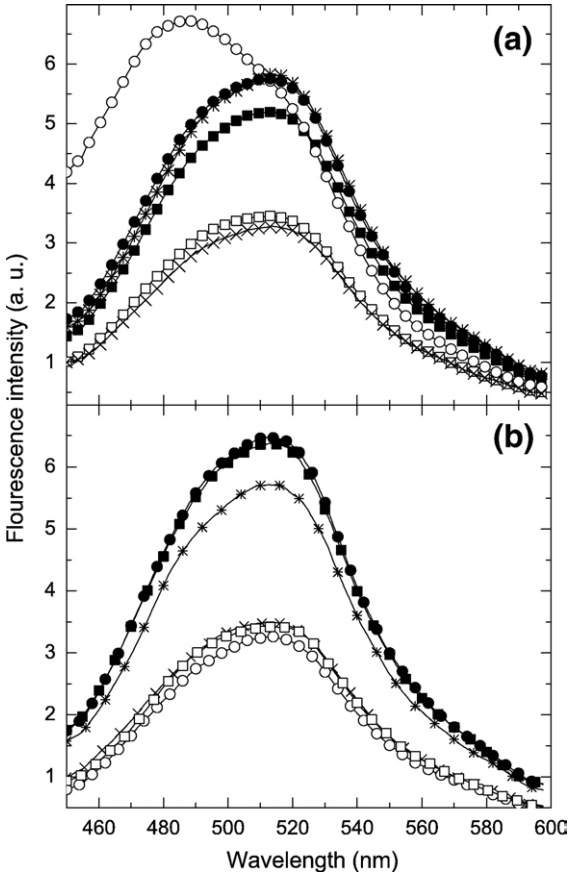

Figure 6. ANS fluorescence emission spectra of (a) Fv fragments and(b) Fab fragments in the absence and in the presence of 8 M urea. Control solutions of PBS (×) and 8 M urea (*). D44.1 fragments in PBS (○), in 8 M urea (●). F10.6.6 fragments in PBS (□), in 8 M urea (■). Fv D44.1 has a 21 nm blue-shifted CM with respect to the Fv F10.6.6, indicating that ANS binds differently to both Fvs in native conditions.

served for the Fab fragments, in either native or denatured conditions (Figure 6(b)).

Figure 7 displays the ANS fluorescence emission at 485 nm as a function of the concentration of urea. The ANS binding curve for Fv D44.1 presents a noticeable transition around 2.0 M urea, indicating the loss of structured hydrophobic patches that bind ANS. In contrast, the binding curve corresponding to Fv F10.6.6 shows no transition and a fluorescence emission with a linear dependence on increasing concentrations of urea.

In summary, Fv D44.1 shows an unusual binding to ANS in native conditions, which suggests that this Fv fragment presents hydrophobic patches on its surface that can be the product of a molten globule conformation. This behavior has not been observed in any of the other antibody fragments tested.

Heat capacity changes in the binding of the Fab and Fv fragments to HEL

This particular system of two structurally and genetically related antibodies with a difference of almost 1000 times in affinity offers the possibility to study the evolution of heat capacity change upon binding (ΔC_p) associated with the affinity maturation process. Several studies have defined the heat capacity change as a weak function of temperature and parameterized in terms of changes in solvent-accessible surface area (ΔASA) originated mainly from changes in hydration.[41] Thus, theoretical ΔC_p values of the available structures of the Fab–HEL complexes were calculated taking into account the changes in the buried apolar and polar surface area upon binding to HEL (ΔASA_{apolar} and ΔASA_{polar}, respectively). The theoretical ΔC_p calculations were done using the structural parameterization and the equation (1):[42–44]

$$\Delta C_p = a\Delta ASA_{apolar} + b\Delta ASA_{polar} \quad (1)$$

where $a = 0.45$ and $b = -0.26$ are the elementary apolar and polar contributions per mole of Å^2 in units of cal K^{-1} mol^{-1}.

As expected for protein–protein interactions, the binding ΔC_p shows negative values (Table 6). In the case of the Fv F10.6.6-HEL reaction, the experimental value agrees almost perfectly with that calculated theoretically. However, in the Fv D44.1-HEL reaction the absolute value of the experimental ΔC_p is much higher than that calculated theoretically. Following the conventional interpretation that ΔC_p values are based on hydrophobic interactions, it can be inferred that the Fv D44.1-HEL complex would present a larger hydrophobic surface of interaction in the antibody–antigen interface than the Fv F10.6.6–HEL complex. However, the Fab F10.6.6–HEL complex crystal structure shows an average increase of 9.5% (58.6 Å^2) in ΔASA due to a 16.5% increase in ΔASA_{apolar} (51.0 Å^2), while ΔASA_{polar} increases only 2.3% with respect to Fab D44.1–HEL complex.[26] As a consequence, the high ΔC_p value of Fv D44.1-HEL reaction cannot be attributed to a large hydrophobic contact surface area with the

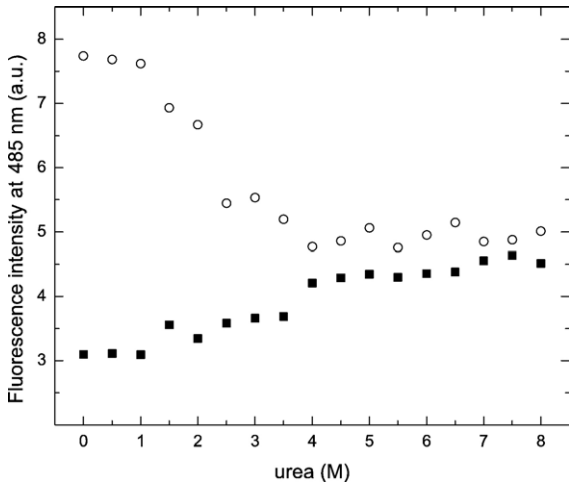

Figure 7. ANS binding in function of urea denaturation. A clear loss of fluorescence is observed for Fv D44.1 (open circles). No significant changes and linear dependence are observed for Fv F10.6.6 (filled squares).

Table 6. Theoretical and experimental binding ΔC_p of the reactions of Fv fragments from mAbs F10.6.6 and D44.1 reactions with HEL

Complex	ΔASA_{apolar} (Å^2)	ΔASA_{polar} (Å^2)	$\Delta C_{p\ theor}$ (cal mol^{-1} K^{-1})	$\Delta C_{p\ exp}$ (cal mol^{-1} K^{-1})
Fv F10.6.6-HEL	−841.9	−614.7	−219.0	−221.5±6.0
Fv D44.1-HEL	−802.5	−589.0	−208.0	−330.1±2.5

ΔASA values of Fv-HEL interface were calculated with NACCESS software, using a probe of 1.4 Å. ΔASA is expressed according to Murphy *et al.*[34]

antigen and to the interactions between non-polar groups in water as it was inferred for other protein–protein complexes.[45,46] Moreover, this discrepancy, although at a lesser extent, is observed also for the reactions of the Fab fragments: Fab D44.1–HEL has a higher negative ΔC_p value (−296.20 cal mol^{-1} K^{-1}) than Fab F10.6.6–HEL reaction (−259.20 cal mol^{1} K^{1}).[47] On the contrary, it appears that the ΔC_p for Fv F10.6.6 fragment binding to HEL is almost exclusively dependent on the apolar and polar surface of interaction. In addition to the absolute values of binding ΔC_p, the loss of linearity of the binding enthalpy in function of temperature for Fv D44.1-HEL reaction at 35 °C and for Fv F10.6.6-HEL reaction at 45 °C can be observed (Figure 8). The loss of linearity in that function in the Fv fragment reactions emphasizes the strong temperature-dependence of enthalpy and was observed in protein interactions where binding is coupled to folding processes.[48] In concordance with the thermal stability results, the strong temperature-dependence for Fv D44.1-HEL is more evident than in Fv F10.6.6-HEL reaction as the curvature appears below physiological temperatures. Conversely, for Fab/IgG-HEL reaction of both antibodies the linearity is conserved until 50 °C,[47] suggesting that for Fv fragments, the lack of constant domain stabilization leads to a mechanism of binding coupled to folding process, especially for Fv D44.1-HEL reaction. This fact is translated into the anomalous binding ΔC_p value of the latter reaction. Therefore, the more unstable the protein, the higher the temperature-dependence of the binding enthalpy.[44,46,49,50]

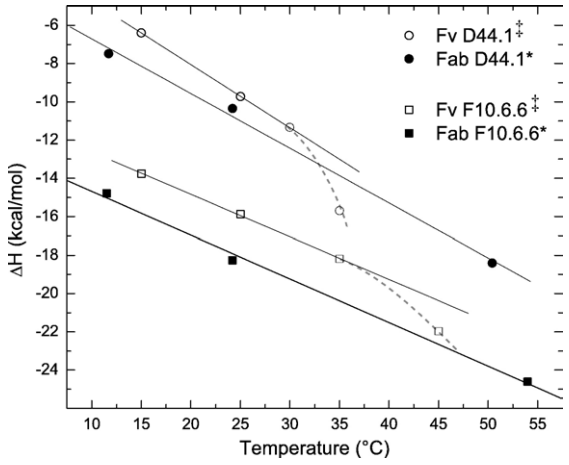

Figure 8. Determination of binding ΔC_p ΔH as a function of temperature is depicted. Fvs data were obtained for this work (‡), Fabs data (*) were published earlier.[47] The loss of linearity of the binding ΔH in function of temperature (broken lines) for Fv D44.1-HEL reaction at 35 °C and for Fv F10.6.6-HEL reaction at 45 °C is observed.

Discussion

The affinity maturation process comprises the introduction of random mutations into rearranged Ig V genes followed by antigen-driven selection of high-affinity clones. In this fashion, the LB clones with higher affinity that possess the best antigen-combing site are selected. In the F10.6.6-D44.1 system, the increase in affinity arises from the combination of several factors, including improved shape complementarity and the resulting additional interfacial hydrogen bonds, vdW contacts and increased *BSA*.[26] All these events are the product of the induced–fit mechanism[4] used to improve the binding towards antigen. This binding mechanism is based on the fact that the Fv domain of mAb F10.6.6 is flexible enough to accommodate the antigen, producing conformational changes that are translated in rmsd values particularly for V_H domains. The concerted combination of local conformational changes at the V_H domain and the quaternary structural changes at V_H–V_L interface accompanied with some changes at paratope side-chains, causes the binding site to broaden and to change shape to improve the antibody complementarity to antigen. Even if the quaternary changes can be considered restrained, the Fab F10.6.6 V_H–V_L interface is sufficiently stable to undergo such changes. Conversely, for Fab D44.1 with lower affinity towards HEL, the mode of binding cannot be described as an induced fit. The combination of the insignificant loss of atomic contacts at the V_H–V_L interface upon binding to antigen, showing global small conformational changes at all V_H structure suggests a less solid organization. This fact suggests the incapacity of this antibody to accommodate the antigen with good complementarity and seems to be the product of a relative unstable V_H–V_L interface in the free form, as was corroborated by CD, DLS and fluorescence experiments. The study of the antibody V_H–V_L interface is gaining attention in many areas of biotechnology, including diagnostics and therapy, because Fv fragments can be produced with relative simplicity by many systems, including microbial

culture. It has been described that FR mutations have important roles in structure preservation, folding yield and stability which, collectively affect affinity.[51,52] Recently, some authors have described the importance of the residues of the FR2 from both V_H and V_L in the V_H–V_L interaction strength and antigen binding affinity.[53] They found that a glutamine residue in position 39 at V_H is crucial in both interactions. In our system composed of F10.6.6 and D44.1 antibodies, both possess such a residue at V_H, but it does not form a hydrogen bond with $Tyr87_L$ as was observed in other antibodies. Instead, $Gln39_H$ forms two hydrogen bonds with $Gln38_L$ in the free form of both antibodies but with shorter distances in Fab F10.6.6. However, the difference in the V_H–V_L interaction between both antibodies appears to be due to a differential interaction between the $FR2_H$, the apical region of $CDR3_H$ and N terminus of the $FR4_H$ region with the V_L domain. In addition, conformational changes at the V_H–V_L interface induced by antigen provides once again experimental evidence for the interface adaptor hypothesis proposed by Colman.[54] This hypothesis is fulfilled by the Fab 50.1, which recognizes a peptide antigen and was described in detail by Stanfield *et al*.[5] In that work, the authors analyzed the quaternary changes and rearrangements at the V_H–V_L interface that accompany antigen binding, relating the observed changes to antigen affinity. The induced-fit mechanism of antigen binding has shown to involve, in some cases, rotation/translation of the V_H–V_L disposition.[5] These changes of the V_H–V_L disposition between several free and bound Fabs fall into the range of 0.7–16.3° and 0.2–2.8 Å, respectively. In the case of Fab F10.6.6. there is a rotation of 2.9° and a translation of 1.1 Å, and for the Fab D44.1, a rotation of 3.0° with a negligible translation. These values are near the lower limit in comparison with all studied antibodies; however, a slightly difference in translation between F10.6.6 and D44.1 is observed, which is in agreement with the loss of atomic contacts. Moreover, as shown by Stanfield *et al*.,[5] the size of the V_H–V_L contact area correlates with the size of the CDR loops, particularly of the $CDR3_H$. This loop in F10.6.6 and D44.1 antibodies has the same length (seven residues), and in both antibodies the *BSA* values of the V_H–V_L interface (measured with the same probe that was used by Stanfield *et al*.[5]) do not correlate with the $CDR3_H$ length, nor do they follow the tendency observed in that work. Thus, for F10.6.6 and D44.1 antibodies, higher V_H–V_L interface *BSA* values are observed in comparison with other antibodies with $CDR3_H$ of the same length.

The structural binding characteristics of F10.6.6 and D44.1 antibodies are translated into thermodynamics of binding: for F10.6.6-HEL reactions, higher enthalpies are observed for both Fv and Fab fragments due to the presence of more and better contacts in the antigen–antibody interface. These favorable contacts are the product of quaternary changes and rearrangements at the V_H–V_L interface. However, the Fv F10.6.6–HEL reaction is one order lower in affinity constant that those for Fab–HEL, because of the lack of the stabilizing constant domain as was described in other antibody–HEL complexes.[20,55] On the contrary, the Fv D44.1–HEL reaction has an affinity constant similar to that of the Fab fragment, demonstrating that for Fv D44.1 structure small rearrangements, if present, do not affect affinity. However, the study of thermal and chemical stability of Fv and Fab fragments of both antibodies by CD, DLS and fluorescence suggests a strong stabilization of the constant domain,[23,56] more noticeable for the Fv D44.1 fragment. Since, during the affinity maturation of F10.6.6 most mutations occur at the V_H domain (especially at the FR regions),[16] the cooperativity observed in the unfolding process of Fv F10.6.6 is due to the stabilizing effects of these mutations. The stability of the Fv fragment of both antibodies agrees with the secondary structure content calculated by analyzing CD spectra, the unfolding pathway and the ANS binding, suggesting that hydrophobic patches are displayed on the surface of Fv D44.1 due to a possible molten globule structure. Although the Fab fragments of both antibodies do not bind ANS, the presence of hydrophobic patches on the surface in the complexed form of Fab D44.1 was stated by Braden *el al*.[25] In that work, buried "holes" at the Fab D44.1-HEL interface situated in a hydrophobic environment of the V_H side-chains were described. Additionally, this particular model of two structurally and genetically related antibodies offers the possibility of studying the evolution of the heat capacity of binding (ΔC_p) linked to the affinity maturation process. In the past, ΔC_p studies of protein–protein interaction attributed the large negative values almost exclusively to a hydrophobic effect.[57,58] This effect results from the formation of cages of structured water of abnormally high heat capacity and low entropy around non-polar groups.[59,60] In fact, as described,[60] the sources of ΔC_p and entropy are numerous and diverse: electrostatic changes, hydrogen bonds, conformational entropy, intramolecular vibrations, changes in equilibria, among others, being much more ubiquitous than has been assumed. In this work, the experimental value of ΔC_p for the Fv F10.6.6–HEL reaction was coincident with the theoretical value calculated from the Murphy and Freire equation,[43] taking into account the polar and non-polar surfaces of interaction. Similar results were reported for the HyHEL-5–HEL reaction[61] ($\Delta C_p = -340$ cal mol^{-1} K^{-1}) suggesting that ΔC_p for F10.6.6 and HyHEL reactions is strongly dependent on the surface of interaction. HyHEL-5 recognizes an epitope that overlaps with that recognized by F10.6.6 and D44.1[25,26,62] with an affinity constant of 4×10^{10} M^{-1}. Its association is accompanied by a favorable enthalpy change and an unfavorable entropy[61] at the temperature assayed for F10.6.6 and D44.1 (see Results). It is important to emphasize that the three antibodies F10.6.6, D44.1 and HyHEL-5 share a basic V sequence, derived from the same V_H gene

recombined with different D (diversity) segments, having a markedly different $CDR3_H$ in the case of HyHEL-5. Therefore, in both high-affinity reactions (F10.6.6–HEL and HyHEL-5–HEL), enthalpy–entropy compensation occurs unlike in the case of D44.1-HEL reaction. This "thermodynamic homeostasis" confers thermodynamic stability and buffering against mutational challenges,[63] that may be of a significant advance in the evolution of protein–ligand systems and in the antibody affinity maturation.

The curvature observed in binding enthalpy as a function of temperature for the Fv D44.1–HEL reaction suggests strongly that the binding is coupled to a folding process. Thus, the molten globule structure can add a component to the enthalpy of binding that is not present in conventional protein–protein interactions. However, that folding component of ΔC_p is not simple to calculate, since the thermal and chemical unfolding curves of Fv D44.1 show a non-cooperative process as part of the native state that is not well defined.

As a general conclusion, the results obtained with our experimental model suggest that the affinity maturation process of anti-protein antibodies - affects the shape of the combining site that recognizes the antigen. This process also affects the secondary structure content of the variable domain, strengthens the V_H–V_L interaction, and consequently increases the plasticity and stability of the Fv domain. At the same time, all these conformational changes improve the binding to antigen. In the future, other experimental models of antibody–protein interactions will assess the generality of the structural mechanism proposed here. Besides, a detailed dissection of binding kinetics and thermodynamics as well as stability is currently being performed using chain shuffling experiments and mutants that represent intermediates between D44.1 and F10.6.6 Fv fragments. These studies will hopefully shed light on the structural mechanisms that follow the fine-tuning of the complementarity of the antigen-combining site towards the epitope.

Materials and Methods

Production of recombinant Fv fragments

The two variable domains V_L and V_H of the Fv fragments of both antibodies D44.1 and F10.6.6 were amplified separately from the cDNA obtained from hybridoma cells. Each variable domain was cloned into the pET22b(+) expression vector, neither pelB signal peptide nor HisTag was used. *Escherichia coli* strain BL21 (DE3) cells were transformed with these constructions to achieve protein expression. Each variable domain was produced by culturing (in shake flasks) appropiately transformed *E. coli* bacteria in Luria-Bertani (LB) medium with 100 μg/ml of ampicilin and induced with 1 mM IPTG for 4 h at 37 °C. Cultures were centrifuged at 4000 g and the bacterial pellets were suspended in one-tenth culture volume with 50 mM Tris–HCl (pH 8.0), 0.5 mM EDTA, 1% (v/v) Triton X-100. Cells were disrupted by sonication and inclusion bodies for each chain were washed twice with 50 mM Tris–HCl (pH 8.0), 0.5 mM EDTA, 1% Triton X-100 and once with this buffer without detergent. To carry out the refolding of the Fvs, inclusion bodies were solubilized in 8 M urea, V_L and V_H solutions were mixed in a 1:1 molar ratio as estimated by SDS-PAGE. Three steps of dialysis against PBS at 4 °C were performed, two steps of 4 h and then one overnight. Refolded Fv fragments were purified by affinity chromatography using an HEL–Sepharose affinity column, washing with several volumes of PBS, 0.5 M NaCl, and eluting active recombinant Fvs with 50 mM diethylamine. The eluate was collected over 1 ml of 0.5 M Tris–HCl (pH 8.0). The presence of the Fvs was checked by SDS-PAGE, and subsequently these fragments were purified by gel-filtration chromatography on a Superdex 75 column (General Electric (GE) Healthcare Life Sciences).

Production of Fab fragments

Fab fragments were obtained as described.[26]

Measurements of kinetic constants by biosensor

Affinity sensor analysis experiments were carried out as described,[26] with an IAsys Plus apparatus (Affinity Sensors, Saxon Hill, Cambridge, UK). Lysozyme was covalently coupled to carboxymethyl dextran sensor chips (Affinity Sensors) giving 5 ng of protein/cuvette. Ligate binding to immobilized ligand was monitored at multiple concentrations of ligand. Kinetic analysis was performed with FASTFIT software (Affinity Sensors, Saxon Hill, Cambridge, UK).

Measurement of thermodynamic binding parameters

The thermodynamic parameters for the binding of Fv D44.1–HEL and Fv F10.6.6–HEL reactions were determined by isothermal calorimetry using a MicroCal VP-ITC titration microcalorimeter (MicroCal). Purified Fvs and HEL (Sigma) were dialysed exhaustively against PBS. In a typical experiment, 3.0–5.0 μl aliquots of 0.3–0.9 mM HEL were injected from a 300 μl rotating syringe at 290 rpm into the sample cell containing 1.47 ml of 0.013–0.030 mM Fv. A non-linear least-squares fitting method was used to determine ΔH, the equilibrium association constant (K_A), and the molar stoichiometry (n). Reversible equilibrium thermodynamics was assumed in calculating values of ΔG, from the relationship $\Delta G = -RT\ln K_A$. The ΔS was calculated from $\Delta G = \Delta H - T\Delta S$. Data acquisition and analysis was done with the software package Origin provided by the manufacturer. The value of ΔC_p was determined from the temperature-dependence of the binding enthalpy. Enthalpy values were measured at different temperatures ranging from 15 °C to 45 °C. Linear least-squares fits were performed with Microcal Origin, and the slope of the adjusted linear function was taken as the measured ΔC_p.

Circular dichroism

Far-UV CD spectra were measured with a Jasco J810 spectropolarimeter using Fv and Fab solutions at concentrations of 20 μM and 8 μM, respectively. Thermal denaturation was conducted by slowly increasing the

temperature with a Peltier system (Jasco). The range of temperature scanning was 5–95 °C at a rate of 2 deg.C/min. Elipticity at 216 nm was measured every 0.5 deg.C. Fast or slow cooling to 25 °C did not show a recovery of elipticity, demonstrating the irreversibility of the thermal unfolding. Thus, the temperature midpoint of the thermal transition was considered as an apparent T_m.

Dynamic light-scattering (DLS)

DLS of the free Fv and Fab fragments were measured with a Malvern ZetaSizer Nano-S apparatus. The concentration of protein was 20 μM for Fvs and 10 μM for Fabs in PBS buffer. Thermal denaturation was conducted by slowly increasing the temperature with the Peltier system. The range of temperature scanning was 30–90 °C at a rate of 1 deg.C/min. Each data point was averaged from six measures of 5 s each. Fast or slow cooling to 30 °C did not show a recovery of original signal of scattering, a confirmation of the irreversibility of the thermal unfolding. Thus, the temperature midpoint of the thermal transition was considered as an apparent T_m. All parameters were used as default.

Fluorescence

Tryptophan intrinsic fluorescence and ANS binding were measured with an LS 50B Perkin Elmer luminescence spectrometer. The concentration of Fvs solutions was 1.0 μM in all cases, using a 4 nm band-pass for excitation and emission slits in all experiments; 50 μM ANS was used with the excitation wavelength setting at 380 nm and spectra were recorded from 450 nm to 600 nm. All spectra were recorded at 25 °C in PBS buffer (pH 7.4).

Crystallization, data collection and processing and structure resolution

The free Fab fragment from the F10.6.6 antibody was crystallized in the monoclinic *C*2 space group by the hanging-drop method using 0.1 M sodium acetate buffer (pH 4.70), 24% (w/v) PEG 1000, 0.2 M $CaCl_2$. Large prisms of about 0.30 mm × 0.05 mm × 0.05 mm were obtained after several weeks. Free Fab F10.6.6 crystals were soaked in their mother liquor with glycerol added to 14% (v/v) and subjected to flash-cooling at 100 K in a stream of nitrogen before data collection. The final native dataset was collected at the D03B-MX1 protein crystallography beamline at the Laboratório Nacional de Luz Síncrotron (LNLS), Brazil,[64] with an MarCCD 165 mm detector and λ = 1.431 Å. A total of 380 frames were collected with 1° oscillation, yielding a highly redundant complete dataset at 2.0 Å (Table 7). Diffraction data were processed with the HKL2000 suite,[65] and phased by molecular replacement with AMoRe,[66] using the Fab model of the complex F10.6.6-HEL (PDB code 1P2C) as the search model.[26] There were two molecules in the asymmetric unit. Refinement was carried out with CNS,[67] with the maximum likelihood algorithm using cycles of simulated annealing. Model building was performed with TURBO†. We arrived at a final model with $R = 0.196$ and $R_{free} = 0.233$ with good geometry (Table 7).

† http://www.afmb.univ-mrs.fr/-TURBO-

Table 7. X-ray data collection parameters and processing and refinement statistics for the free Fab F10.6.6 structure

A. *Data collection*	
No. frames	380
Oscillation step (deg)	1
Wavelength (Å)	1.431
B. *Indexing and scaling*	
Cell parameters: *a*, *b*, *c* (Å)	108.76, 80.25, 91.50
Cell angles: α, β, γ (deg.)	90, 91.50, 90
Space group	*C*2
Resolution limit (Å)	2.00
Total reflections	401,430
No. unique reflections	50,300
Multiplicity[a]	8.1 (8.2)
I/σ	9.8 (3.3)
R_{merge} (%)[b]	6.9 (19.5)
Completeness (%)	96.0 (92.0)
Molecules / asymmetric unit	2
Solvent content (%)	41.0
Matthews coefficient (Å^3/Da)	2.1
C. *Refinement*	
Resolution limits (Å)	20.0–2.00
R-factor	0.196
Free *R*-factor	0.233
Non-hydrogen protein atoms	6486
No. solvent molecules	518
r.m.s.d. bond lengths (Å)	0.006
r.m.s.d. bond angles (deg)	1.41
Average *B*-factor (Å^2)	22.0
Ramachandran plot	
Most favored regions (%)	88.7
Additionally allowed regions (%)	10.2
Generously allowed regions (%)	0.7
Disallowed regions (%)	0.4

[a] Values in parentheses correspond to the highest resolution shell (2.07–2.00 Å).
[b] $R_{merge} = [\sum_i | I_i - \langle I \rangle | / \sum_i I_i]$.

Structural analysis

Water molecules displacement was calculated taking into account water molecules with *B*-factors <40 Å^2 that form hydrogen bonds with antibody residues that interact with HEL at a distance <7 Å (two hydrogen bonds distance).

Protein Data Bank accession codes

The atomic coordinates and structure factors have been deposited in the RCSB Protein Data Bank and are available under accession code 2Q76.

Acknowledgements

This work was supported by a Fogarty International Research Collaboration Award grant from the Fogarty International Center, National Institutes of Health (to B.C.B and F.A.G.), and by a grant from the National Scientific and Technological Research Council of Argentina (CONICET PIP 6171, to A.A.C.). We received financial assistance from the Laboratório

Nacional de Luz Síncrotron (LNLS) under project number D03B-CPR-1801.

Supplementary Data

Supplementary data associated with this article can be found, in the online version, at doi:10.1016/j.jmb.2007.09.005

References

1. Roost, H. P., Bachmann, M. F., Haag, A., Kalinke, U., Pliska, V., Hengartner, H. & Zinkernagel, R. M. (1995). Early high-affinity neutralizing anti-viral IgG responses without further overall improvements of affinity. *Proc. Natl Acad. Sci. USA*, **92**, 1257–1261.
2. England, P., Nageotte, R., Renard, M., Page, A. L. & Bedouelle, H. (1999). Functional characterization of the somatic hypermutation process leading to antibody D1.3, a high affinity antibody directed against lysozyme. *J. Immunol.* **162**, 2129–2136.
3. Bhat, T. N., Bentley, G. A., Boulot, G., Greene, M. I., Tello, D., Dall'Acqua, W. *et al.* (1994). Bound water molecules and conformational stabilization help mediate an antigen-antibody association. *Proc. Natl Acad. Sci. USA*, **91**, 1089–1093.
4. Rini, J. M., Schulze-Gahmen, U. & Wilson, I. A. (1992). Structural evidence for induced fit as a mechanism for antibody-antigen recognition. *Science*, **255**, 959–965.
5. Stanfield, R. L., Takimoto-Kamimura, M., Rini, J. M., Profy, A. T. & Wilson, I. A. (1993). Major antigen-induced domain rearrangements in an antibody. *Structure*, **1**, 83–93.
6. Foote, J. & Eisen, H. N. (1995). Kinetic and affinity limits on antibodies produced during immune responses. *Proc. Natl Acad. Sci. USA*, **92**, 1254–1256.
7. Batista, F. D. & Neuberger, M. S. (1998). Affinity dependence of the B cell response to antigen: a threshold, a ceiling, and the importance of off-rate. *Immunity*, **8**, 751–759.
8. Foote, J. & Milstein, C. (1991). Kinetic maturation of an immune response. *Nature*, **352**, 530–532.
9. Foote, J. & Winter, G. (1992). Antibody framework residues affecting the conformation of the hypervariable loops. *J. Mol. Biol.* **224**, 487–499.
10. Wedemayer, G. J., Patten, P. A., Wang, L. H., Schultz, P. G. & Stevens, R. C. (1997). Structural insights into the evolution of an antibody combining site. *Science*, **276**, 1665–1669.
11. Scotti, C. & Gherardi, E. (2006). Structural basis of affinity maturation of the TEPC15/Vkappa45.1 anti-2-phenyl-5-oxazolone antibodies. *J. Mol. Biol.* **359**, 1161–1169.
12. Yin, J., A.E.t. Beuscher, S. E., Andryski, R. C. & Stevens, P. G. (2003). Structural plasticity and the evolution of antibody affinity and specificity. *J. Mol. Biol.* **330**, 651–656.
13. Furukawa, K., Shirai, H., Azuma, T. & Nakamura, H. (2001). A role of the third complementarity-determining region in the affinity maturation of an antibody. *J. Biol. Chem.* **276**, 27622–27628.
14. Zimmermann, J., Oakman, E. L., Thorpe, I. F., Shi, X., Abbyad, P., Brooks, C. L., III *et al.* (2006). Antibody evolution constrains conformational heterogeneity by tailoring protein dynamics. *Proc. Natl Acad. Sci. USA*, **103**, 13722–13727.
15. Thorpe, I. F. & Brooks, C. L., III (2007). Molecular evolution of affinity and flexibility in the immune system. *Proc. Natl Acad. Sci. USA*, **104**, 8821–8826.
16. Goldbaum, F. A., Cauerhff, A., Velikovsky, C. A., Llera, A. S., Riottot, M. M. & Poljak, R. J. (1999). Lack of significant differences in association rates and affinities of antibodies from short-term and long-term responses to hen egg lysozyme. *J. Immunol.* **162**, 6040–6045.
17. Li, Y., Li, H., Yang, F., Smith-Gill, S. J. & Mariuzza, R. A. (2003). X-ray snapshots of the maturation of an antibody response to a protein antigen. *Nature Struct. Biol.* **10**, 482–488.
18. Milstein, C. & Rada, C. (1995). The maturation of the antibody response. In *Immunoglobulin Genes* (Honjo, T. & Alt, F. W., eds), 2nd edit., Academic Press, London.
19. Monaco-Malbet, S., Berthet-Colominas, C., Novelli, A., Battai, N., Piga, N., Cheynet, V. *et al.* (2000). Mutual conformational adaptations in antigen and antibody upon complex formation between an Fab and HIV-1 capsid protein p24. *Structure*, **8**, 1069–1077.
20. Bhat, T. N., Bentley, G. A., Fischmann, T. O., Boulot, G. & Poljak, R. J. (1990). Small rearrangements in structures of Fv and Fab fragments of antibody D1.3 on antigen binding. *Nature*, **347**, 483–485.
21. Kondo, H., Shiroishi, M., Matsushima, M., Tsumoto, K. & Kumagai, I. (1999). Crystal structure of anti-Hen egg white lysozyme antibody (HyHEL-10) Fv-antigen complex. Local structural changes in the protein antigen and water-mediated interactions of Fv-antigen and light chain-heavy chain interfaces. *J. Biol. Chem.* **274**, 27623–27631.
22. Padlan, E. A., Silverton, E. W., Sheriff, S., Cohen, G. H., Smith-Gill, S. J. & Davies, D. R. (1989). Structure of an antibody-antigen complex: crystal structure of the HyHEL-10 Fab-lysozyme complex. *Proc. Natl Acad. Sci. USA*, **86**, 5938–5942.
23. Rothlisberger, D., Honegger, A. & Pluckthun, A. (2005). Domain interactions in the Fab fragment: a comparative evaluation of the single-chain Fv and Fab format engineered with variable domains of different stability. *J. Mol. Biol.* **347**, 773–789.
24. Jager, M. & Pluckthun, A. (1999). Folding and assembly of an antibody Fv fragment, a heterodimer stabilized by antigen. *J. Mol. Biol.* **285**, 2005–2019.
25. Braden, B. C., Souchon, H., Eisele, J. L., Bentley, G. A., Bhat, T. N., Navaza, J. & Poljak, R. J. (1994). Three-dimensional structures of the free and the antigen-complexed Fab from monoclonal anti-lysozyme antibody D44.1. *J. Mol. Biol.* **243**, 767–781.
26. Cauerhff, A., Goldbaum, F. A. & Braden, B. C. (2004). Structural mechanism for affinity maturation of an anti-lysozyme antibody. *Proc. Natl Acad. Sci. USA*, **101**, 3539–3544.
27. Alzari, P. M., Spinelli, S., Mariuzza, R. A., Boulot, G., Poljak, R. J., Jarvis, J. M. & Milstein, C. (1990). Three-dimensional structure determination of an anti-2-phenyloxazolone antibody: the role of somatic mutation and heavy/light chain pairing in the maturation of an immune response. *EMBO J.* **9**, 3807–3814.
28. Yang, P. L. & Schultz, P. G. (1999). Mutational analysis of the affinity maturation of antibody 48G7. *J. Mol. Biol.* **294**, 1191–1201.
29. Kabsch, W. & Sander, C. (1983). Dictionary of protein secondary structure: pattern recognition of hydrogen-bonded and geometrical features. *Biopolymers*, **22**, 2577–2637.
30. Azuma, T., Hamaguchi, K. & Migita, S. (1972). Denaturation of Bence Jones proteins by guanidine hydrochloride. *J. Biochem. (Tokyo)*, **72**, 1457–1467.

31. Tetin, S. Y. & Linthicum, D. S. (1996). Circular dichroism spectroscopy of monoclonal antibodies that bind a superpotent guanidinium sweetener ligand. *Biochemistry*, **35**, 1258–1264.
32. Espeso, E. A. & Penalva, M. A. (1994). In vitro binding of the two-finger repressor CreA to several consensus and non-consensus sites at the ipnA upstream region is context dependent. *FEBS Letters*, **342**, 43–48.
33. Yasui, H., Ito, W. & Kurosawa, Y. (1994). Effects of substitutions of amino acids on the thermal stability of the Fv fragments of antibodies. *FEBS Letters*, **353**, 143–146.
34. Tetin, S. Y., Prendergast, F. G. & Venyaminov, S. Y. (2003). Accuracy of protein secondary structure determination from circular dichroism spectra based on immunoglobulin examples. *Ana. Biochem.* **321**, 183–187.
35. Tetin, S., Mantulin, W. W., Denzin, L. K., Weidner, K. M. & Voss, E. W., Jr (1992). Comparative circular dichroism studies of an anti-fluorescein monoclonal antibody (Mab 4-4-20) and its derivatives. *Biochemistry*, **31**, 12029–12034.
36. Sreerama, N. & Woody, R. W. (2000). Estimation of protein secondary structure from circular dichroism spectra: comparison of CONTIN, SELCON, and CDSSTR methods with an expanded reference set. *Anal. Biochem.* **287**, 252–260.
37. Privalov, P. L. (1996). Intermediate states in protein folding. *J. Mol. Biol.* **258**, 707–725.
38. Stryer, L. (1965). The interaction of a naphthalene dye with apomyoglobin and apohemoglobin. A fluorescent probe of non-polar binding sites. *J. Mol. Biol.* **13**, 482–495.
39. Semisotnov, G. V., Rodionova, N. A., Razgulyaev, O. I., Uversky, V. N., Gripas, A. F. & Gilmanshin, R. I. (1991). Study of the "molten globule" intermediate state in protein folding by a hydrophobic fluorescent probe. *Biopolymers*, **31**, 119–128.
40. Kuwajima, K. (1989). The molten globule state as a clue for understanding the folding and cooperativity of globular-protein structure. *Proteins: Struct. Funct. Genet.* **6**, 87–103.
41. Luque, I. & Freire, E. (1998). Structure-based prediction of binding affinities and molecular design of peptide ligands. *Methods Enzymol.* **295**, 100–127.
42. Murphy, K. P., Bhakuni, V., Xie, D. & Freire, E. (1992). Molecular basis of co-operativity in protein folding. III. Structural identification of cooperative folding units and folding intermediates. *J. Mol. Biol.* **227**, 293–306.
43. Murphy, K. P. & Freire, E. (1992). Thermodynamics of structural stability and cooperative folding behavior in proteins. *Advan. Protein Chem.* **43**, 313–361.
44. Murphy, K. P., Xie, D., Garcia, K. C., Amzel, L. M. & Freire, E. (1993). Structural energetics of peptide recognition: angiotensin II/antibody binding. *Proteins: Struct. Funct. Genet.* **15**, 113–120.
45. Cooper, A. (2005). Heat capacity effects in protein folding and ligand binding: a re-evaluation of the role of water in biomolecular thermodynamics. *Biophys. Chem.* **115**, 89–97.
46. Spolar, R. S. & Record, M. T., Jr (1994). Coupling of local folding to site-specific binding of proteins to DNA. *Science*, **263**, 777–784.
47. Schwarz, F. P., Tello, D., Goldbaum, F. A., Mariuzza, R. A. & Poljak, R. J. (1995). Thermodynamics of antigen-antibody binding using specific anti-lysozyme antibodies. *Eur. J. Biochem.* **228**, 388–394.
48. Cliff, M. J., Williams, M. A., Brooke-Smith, J., Barford, D. & Ladbury, J. E. (2005). Molecular recognition via coupled folding and binding in a TPR domain. *J. Mol. Biol.* **346**, 717–732.
49. Bowie, J. U. & Sauer, R. T. (1989). Equilibrium dissociation and unfolding of the Arc repressor dimer. *Biochemistry*, **28**, 7139–7143.
50. Jin, L., Yang, J. & Carey, J. (1993). Thermodynamics of ligand binding to trp repressor. *Biochemistry*, **32**, 7302–7309.
51. David, M. P., Asprer, J. J., Ibana, J. S., Concepcion, G. P. & Padlan, E. A. (2007). A study of the structural correlates of affinity maturation: antibody affinity as a function of chemical interactions, structural plasticity and stability. *Mol. Immunol.* **44**, 1342–1351.
52. Jung, S., Spinelli, S., Schimmele, B., Honegger, A., Pugliese, L., Cambillau, C. & Pluckthun, A. (2001). The importance of framework residues H6, H7 and H10 in antibody heavy chains: experimental evidence for a new structural subclassification of antibody V(H) domains. *J. Mol. Biol.* **309**, 701–716.
53. Masuda, K., Sakamoto, K., Kojima, M., Aburatani, T., Ueda, T. & Ueda, H. (2006). The role of interface framework residues in determining antibody V(H)/V(L) interaction strength and antigen-binding affinity. *FEBS J.* **273**, 2184–2194.
54. Colman, P. M. (1988). Structure of antibody-antigen complexes: implications for immune recognition. *Advan. Immunol.* **43**, 99–132.
55. Padlan, E. A. (1994). Anatomy of the antibody molecule. *Mol. Immunol.* **31**, 169–217.
56. Lilie, H. & Buchner, J. (1995). Domain interactions stabilize the alternatively folded state of an antibody Fab fragment. *FEBS Letters*, **362**, 43–46.
57. Kauzmann, W. (1959). Some factors in the interpretation of protein denaturation. *Advna. Protein Chem.* **14**, 1–63.
58. Sigurskjold, B. W. & Bundle, D. R. (1992). Thermodynamics of oligosaccharide binding to a monoclonal antibody specific for a Salmonella O-antigen point to hydrophobic interactions in the binding site. *J. Biol. Chem.* **267**, 8371–8376.
59. Kuntz, I. D., Jr & Kauzmann, W. (1974). Hydration of proteins and polypeptides. *Advan. Protein Chem.* **28**, 239–345.
60. Sturtevant, J. M. (1977). Heat capacity and entropy changes in processes involving proteins. *Proc. Natl Acad. Sci. USA*, **74**, 2236–2240.
61. Hibbits, K. A., Gill, D. S. & Willson, R. C. (1994). Isothermal titration calorimetric study of the association of hen egg lysozyme and the anti-lysozyme antibody HyHEL-5. *Biochemistry*, **33**, 3584–3590.
62. Sheriff, S., Silverton, E. W., Padlan, E. A., Cohen, G. H., Smith-Gill, S. J., Finzel, B. C. & Davies, D. R. (1987). Three-dimensional structure of an antibody-antigen complex. *Proc. Natl Acad. Sci. USA*, **84**, 8075–8079.
63. Cooper, A., Johnson, C. M., Lakey, J. H. & Nollmann, M. (2001). Heat does not come in different colours: entropy-enthalpy compensation, free energy windows, quantum confinement, pressure perturbation calorimetry, solvation and the multiple causes of heat capacity effects in biomolecular interactions. *Biophys. Chem.* **93**, 215–230.
64. Polikarpov, I., Oliva, G., Castellano, E. E., Garratt, R. C., Arruda, P., Leite, A. & Craievich, A. (1998). The protein crystallography beamline at LNLS, the Brazilian National Synchrotron Light source. *Nucl. Instrum. Methods Phys. Res. A*, **405** (1), 159–164.
65. Otwinowski, Z. & Minor, W. (1997). Processing of X-ray diffraction data collected in oscillation mode. *Methods Enzymol.* **276**, 307–326.

66. Navaza, J. A. C. (1994). AMoRe: an automated package for molecular replacement. *Acta Crystallog. sect. A*, **276**, 157–163.
67. Brunger, A. T., Adams, P. D., Clore, G. M., Delano, W. L., Gros, P. *et al.* (1998). Crystallography and NMR system (CNS): a new software system for macromolecular structure determination. *Acta Crystallog. sect. D*, **54** (5), 905–921.
68. Mitchell, J. C., Kerr, R. & Ten Eyck, L. F. (2001). Rapid atomic density methods for molecular shape characterization. *J. Mol. Graph. Model.* **19**, 325–330.
69. Kabat, E. A. (1978). The structural basis of antibody complementarity. *Advan. Protein Chem.* **32**, 1–75.
70. Kabat, E. A., Wu, T. T. & Bilofsky, H. (1977). Unusual distributions of amino acids in complementarity-determining (hypervariable) segments of heavy and light chains of immunoglobulins and their possible roles in specificity of antibody-combining sites. *J. Biol. Chem.* **252**, 6609–6616.
71. Chothia, C., Lesk, A. M., Tramontano, A., Levitt, M., Smith-Gill, S. J., Air, G. *et al.* (1989). Conformations of immunoglobulin hypervariable regions. *Nature*, **342**, 877–883.